Strain Effects in the Paraelectric Resonance of KCl : Li

B. Dischler

Institut für Angewandte Festkörperphysik der Fraunhofer-Gesellschaft, Freiburg (W.-Germany)

(Z. Naturforsch. **28 a**, 938–952 [1973]; received 3 February 1973)

The effects of random internal strains on the paraelectric resonance spectra for off-center Li in KCl are investigated quantitatively. Diagrams giving the theoretical line positions and relative intensities are presented for the principal orientations ⟨100⟩, ⟨110⟩, and ⟨111⟩. Where the model for an ideal host crystal predicts only one line, up to six lines are obtained in the present calculation. A direct comparison with the published experimental spectra, taken at 9, 24, 29, 35, 63 and 74 GHz is performed. Very good agreement is found and the magnitude of internal strain has been inferred, yielding values between 18 and 42 bar for different samples. Random internal electric fields are found to be of the order 3 kV/cm. For the halfwidth of the main signal, the orientation and frequency dependence is examined and explained by the calculations. The possible use of paraelectric Li as a microprobe for internal strains and internal electric fields in KCl is discussed. The electric dipole moment of Li^7 is found to be 5.9 ± 0.3 Debye in agreement with previous determinations. The "cube edge" tunneling model with equidistant zero field levels, separated by 22.2 GHz for Li^7, is fully confirmed.

Introduction

The physical properties observed for off-center Li in KCl are strongly influenced by random internal strains. In the first article [1] of this series (hereafter referred to as I) the general method for treating strain effects was described, and in particular the effects of strain on the tunneling levels in the absence of external electric fields and applied stress were considered. Earlier [2] we have used the method to explain unexpected details in two particular paraelectric resonance spectra.

The present article analyzes strain effects on the paraelectric resonance (PER) spectra of KCl : Li. The published PER spectra for the ⟨100⟩, ⟨110⟩, ⟨111⟩ orientation will be reviewed. Calculated spectra for these orientations in the frequency range 0 to 90 GHz will be presented, using the internal strain as a free parameter. The strain magnitude in the experimental samples will then be inferred by comparison with the calculations. It will be assumed that the static and microwave electric fields are parallel (the usual experimental configuration), neglecting the one experimental exception [3]. Strain effects in PER spectra taken under applied uniaxial stress [4, 5] will be treated in a subsequent paper [6].

The literature on the system KCl : Li has been briefly reviewed in I (= Ref. [1]). There are several new additions: i) Isofrequency PER measurements for successive frequencies in the range 25 to 64 GHz [7]; ii) Isofield PER measurements for the ⟨100⟩ orientation with transmission microwave techniques and a frequency sweep from 8 to 40 GHz [8]; iii) PER measurements at 74 GHz [4]; iv) Uniaxial stress studies for PER spectra taken at 35 GHz [4] and 58 to 64 GHz [5]; v) PER relaxation time measurements [9]; vi) Far infrared studies [10].

In the following use is made of the well established facts (cf. I) that Li in KCl has eight ⟨111⟩ off-center positions and tunneling occurs only between nearest neighbour positions, i. e. cube edge tunneling.

Reprint requests to Dr. B. Dischler, Institut für Angewandte Festkörperphysik, *D-7800 Freiburg*, BRD (West-Germany), Eckerstr. 4.

1. Ideal versus Real KCl Host

The early theoretical treatments of paraelectric off-center ions [11, 12] or molecular impurities [13] in KCl assumed that the host crystal forms a rigid cage with the full O_h symmetry. With respect to the rigid lattice it was mentioned [11a], that the true behaviour may be that of a coupled dynamic lattice-defect system. The ideal O_h symmetry was questioned by the remark [13a]: "... the calculations are somewhat unrealistic in that they assume an unstrained crystal". Both warnings have been subsequently forgotten. Therefore the PER experimentalists were initially puzzled by the disagreement between theoretical predictions and the observed PER spectra. For KCl : Li this puzzle ended in 1969, when internal strains were introduced into the calculations and satisfactory agreement was obtained [2, 14].

1.1. Ideal Host Crystal

The predicted PER spectra for the case of an ideal host [11, 12] are summarized in Fig. 1. There are two characteristics: i) For each of the principal orientations ⟨100⟩, ⟨110⟩, and ⟨111⟩ only one PER resonance occurs; ii) The zero field splitting constitutes a threshold frequency for PER transitions.

The analytical expression for the resonance condition is

$$(\nu/2\eta)^2 = 1 + d(pF/\eta)^2;\ d>0. \qquad (1)$$

Here the effective Hamiltonian has been used, which was described in I. In Eq. (1) ν is the transition frequency, 2η is the zero field tunnel splitting, p is the electric dipole moment and F is the electric field. The slope coefficient d has the values 1, $^1/_2$, and $^1/_3$ for the ⟨100⟩, ⟨110⟩, and ⟨111⟩ orientation respectively. Consequently the resonance fields in isofrequency spectra for these three orientations must be in the ratio $1 : \sqrt{2} : \sqrt{3}$.

The frequency dependence of the transition probability is given by

$$W(\nu) = (2\eta/\nu)^2 W_0;\ \nu \geqq |2\eta| \qquad (2)$$

and is shown in Figure 1 b. W_0 is the maximum value and occurs at $\nu = |2\eta|$. The inverse proportionality to the square of the frequency is somewhat artificial since the gain by different Boltzman factors has not been considered. This gain is proportional to ν for $h\nu \ll kT$ leading to

$$I(\nu) = (2\eta/\nu) W_0;\ \nu \geqq |2\eta|. \qquad (3)$$

This modified frequency dependence is shown as a broken line in Figure 1 b. Actually PER has been extended to the infrared, where the only limitation has been the dielectric breakdown of KCl under the necessary applied electric field [10].

1.2. Real Host Crystal

In the real KCl host random internal strains are present and their interaction with the elastic moment of the off-center Li is strong enough to modify the PER spectra in a complicated way. To treat the strain as a perturbation would be an economic mathematical method, however during its realization it was found [14], that in the Hamiltonian the elastic energy terms are not small enough in comparison with the electric energy and tunneling terms to yield reliable results.

The numerical diagonalization used in the present paper has been described in I. In order to simulate the random internal strains 13 different directions of uniaxial stress have been selected with statistical weights appropriate to give an isotropic distribution over the unit sphere. The magnitude of the stress is used as the free parameter, expressed in the normalized unit $|qS/\eta|$, where q is the elastic moment, S the stress and η the tunneling parameter (cf. I). The computer program calculates * the positions and relative intensities of the lines in an isofrequency PER spectrum. The total spectrum is obtained by summing over the 13 stress directions and by converting groups of delta-function lines into signals, making use of the moment method described in I.

The results for Li in a real KCl host will be presented in Sections 2.2, 3.2, and 4.2. There are two significant differentes compared to the ideal case of Figure 1: i) Up to three signals for the ⟨100⟩ orientation and up to six signals for the ⟨110⟩ and ⟨111⟩ orientation are predicted. ii) The previous zero field splitting is washed out, and instead of a threshold behaviour, PER spectra continue to exist down to the radio frequency range.

The agreement with experiment is very good and the calculations not only allow a full interpretation of the observed spectra but in addition a careful analysis provides information on the statistics of internal strains.

2. PER for the ⟨100⟩ Orientation

The PER for the ⟨100⟩ orientation has been extensively studied. The signals are sharper than for any other orientation and the samples can be easily prepared since KCl cleaves in {100} planes.

2.1. Observed ⟨100⟩ Spectra

Table 1 is a compilation of data on experimental ⟨100⟩ spectra which have been published [2–4, 14, 15] or are containd in thesis work [16]. In these isofrequency spectra the microwave absorption is measured as a function of the applied electric field F. Usually the authors reproduce the recorder traces, which for experimental reasons give the absorption derivative $\partial\varepsilon''/\partial F$. To prepare Table 1 values of $\partial\varepsilon''/\partial F$ were read of the figures in 1 kV/cm inter-

* Calculations were performed on the IBM 7040 computer of the Rechenzentrum der Universität Freiburg (i. Br.).

Table 1. Data on ⟨100⟩ PER spectra of KCl: Li^7.

Ref.	Experiment				Assignment	Analysis			
	ν (GHz)	$c \cdot F$ (kV/cm)	$2W_h$ (kV/cm)	I_{rel} (%)		$\frac{\nu}{\lvert\eta\rvert}$	$\frac{qS}{\eta}$	new p_{eff} (D)	old p_{eff} (D)
15	35.0	7.8±0.3	6.2	93±5	B	3.15	1.1	6.0	8.6
		16.0±1.0	6.2	7±5	C				
14	63.1	9.7±1.0	4.3	6±3	A	5.69	1.25	5.8	5.6
		17.6±0.4	5.0	86±9	B				
		25.3±1.5	6.0	8±5	C				
	25.16	2.8±1.0	6.0	90±5	B	2.27	1.25	—	—
		12.0±1.5	7.6	10±5	C				
	23.1	1.8±1.0	5.8	82±4	B	2.08	1.25	—	—
		10.0±1.5	7.2	18±4	C				
	9.04	5.6±0.3	5.2	93±3	C	0.81	1.25	—	—
		15.2±0.8	5.6	7±3	D				
2	29.1	6.0±0.8	6.0	81±6	B	2.62	2.5	5.4	6.0
		17.0±0.9	9.5	19±6	C				
16	36.43	8.4±0.5	5.2	88±6	B	3.28	1.7	5.9	5.6
3	34.7	7.4±0.3	3.8	85±5	B	3.13	2.0	6.2	6.3
		16.6±0.8	6.0	15±5	C				
	9.62	1.6±0.4	4.2	53±9	C′	0.87	2.0	—	—
		6.2±0.6	4.2	33±6	C				
		15.0±0.5	6.4	14±5	D				
	9.07	1.2±0.4	4.8	32±9	C′	0.82	2.0	—	—
		6.0±0.5	5.0	52±9	C				
		14.8±0.5	5.5	16±6	D				
	8.91	5.8±0.3	5.0	76±5	C	0.80	2.0	—	—
		14.7±0.5	5.4	24±5	D				
4	72.2	10.8±1.0	6.1	13±5	A	6.51	2.0	5.9	6.0
		20.1±0.4	3.3	70±10	B				
		28.4±1.0	6.5	17±5	C				

Average $p_{eff}=5.9$

vals and integrated numerically. The resulting absorption curves appeared to be distorted by a "background" signal, which in all cases has a dispersion-like shape. The dotted line in Fig. 2 c shows a typical example. Since it is well known that a pure absorption mode is difficult to obtain with PER spectrometers, the assumption of some dispersion signal appears justified and it was decided to subtract this "background". From the corrected absorption curves the resonant field values F, the apparent full width at half height $2W_h$, and the relative integrated intensities I_{rel} were determined.

The entries in Table 1 are grouped by authors and are roughly in chronological order. In order to make the data from different spectra consistent it was necessary to introduce a field calibration coefficient c, where $c=1$ for exact calibration. Accurate experimental field values are obtained only if the field is homogeneous, and the high voltage together with the eletrode distance are known exactly. The actual values of c are not known, however the scattering of the electric dipole moment derived in Table 1 suggests a 0 to 5% deviation of c from 1. In addition to this "systematic" error there is an uncertainty in the determination of the cF values from the spectra, especially for weak or broad signals, and this error is indicated in Table 1. The values for the halfwidth $2W_h$ range from 3.3 to 9.5 kV/cm; they will be discussed later. The relative integrated intensities are given as the percentage of the total intensity in the spectrum.

The columns under the heading "Analysis" make use of the calculated spectra presented in section 2.2 and will be discussed in Section 2.3. Table 1 shows, that three types of spectra have been observed between 9 and 72 GHz. A spectrum with three signals A, B, C, as shown in Figure 2 c, is typical for high frequencies down to 50 GHz, where signal A disappears at zero field [7]. Twno signals B and C are observed from 50 GHz down to 22 GHz,

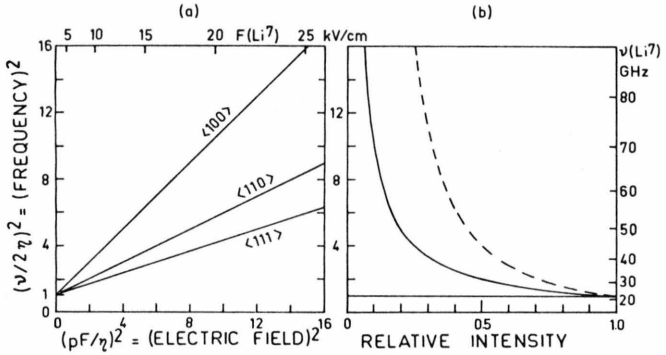

Fig. 1.

Fig. 1. (a) Relation between microwave frequency and applied electric field according to the resonance condition of Equation (1). The orientation of the electric field is indicated by the labels ⟨100⟩, ⟨110⟩, and ⟨111⟩. To obtain these straight lines a double quadratic plot has been used. If Eq. (1) holds, the tunneling frequency and the electric dipole moment can be determined directly from experiment using the intercept and slope of lines in such a plot. Normalized (quadratic) units are used on the left and bottom scale while in the right and top scale the corresponding absolute units are given, appropriate for Li^7 in KCl. (b) Frequency dependence for the relative intensity of the PER transitions shown in Figure 1 a. The solid (hyperbolic) curve gives the transition matrix element according to Equation (2). This curve is equally valid for the three orientaions ⟨100⟩, ⟨110⟩, and ⟨111⟩. The broken curve includes thermal depopulation effects according to Equation (3). The vertical scale coincides with that of Figure 1 a. The bottom scale is linear where $W_0=1$ has been chosen for the maximum intensity.

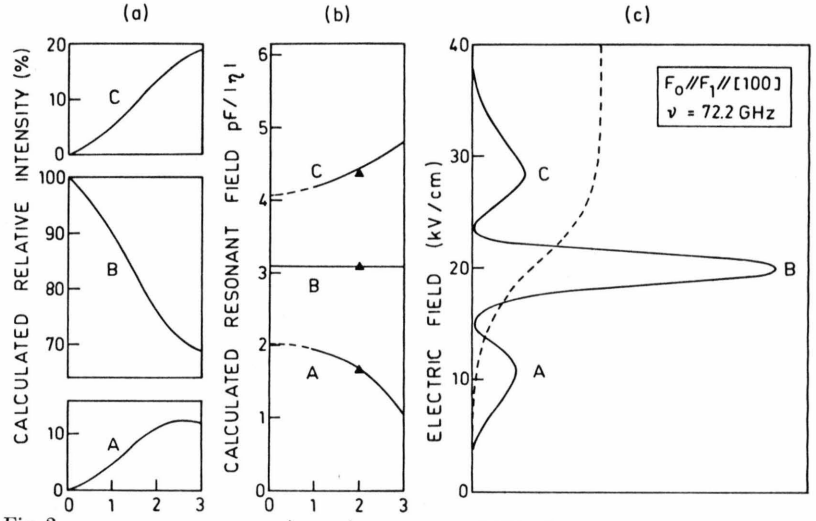

Fig. 2.

Fig. 2. (a) Calculated relative intensities for the PER signals of Fig. 2 b and their dependence on the strain parameter $|qS/\eta|$.
(b) Calculated line positions for a ⟨100⟩ PER spectrum as a function of the strain parameter $|qS/\eta|$. The vertical scale is in normalized field units and coincides with the absolute scale of Figure 2 c. The microwave frequency is 72.2 GHz corresponding to a normalized frequency of $\nu/|\eta|=6.51$.
(c) Experimental PER absorption spectrum after Blumenstock, Osswald and Wolf [4]. The static (F_0) and oscillating (F_1) electric field are along [100] and the frequency is 72.2 GHz. The broken line represents the "background" signal which has been substracted to obtain the solid line (see text).

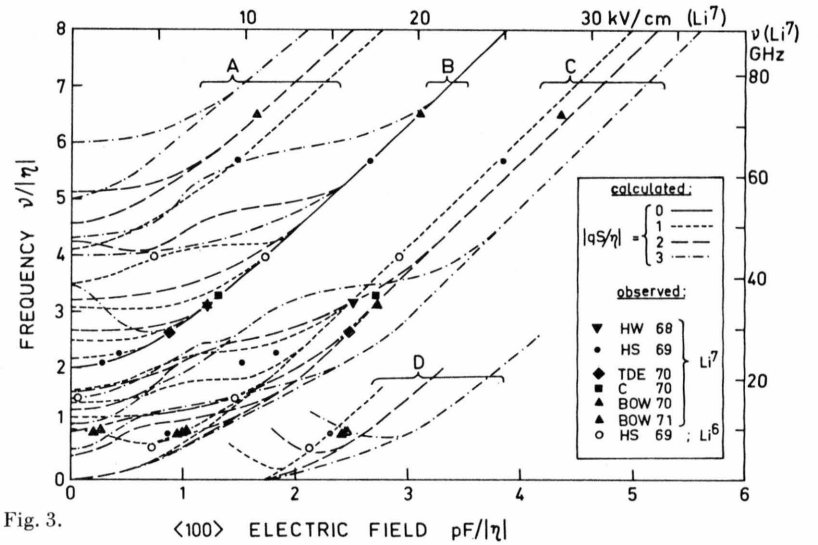

Fig. 3.

Fig. 3. Frequency versus field diagram for ⟨100⟩ PER spectra showing calculated and observed line positions for KCl : Li. The left and bottom scale are in normalized units allowing to include both Li^6 and Li^7 in the same diagram. The corresponding absolute units on the right and top scale are for Li^7 only with $|\eta|=11.1$ GHz and $p_{eff}=5.9$ D. The curves were calculated using values of 0, 1, 2, and 3 for the strain parameter $|qS/\eta|$. They are labelled A, B, C, and D from left to right. Experimental points are given according to Tables 1 and 2. The abbreviations in the insert have the following meaning: HW 68 = [15], HS 69 = [14], TDE 70 = [2b], C 70 = [16], BOW 70 = [3], and Bow 71 = [4].

Table 2. Data on ⟨100⟩ PER spectra of KCl: Li^6.

Ref.	Experiment				Assignment	Analysis			
	ν (GHz)	$c \cdot F$ (kV/cm)	$2W_h$ (kV/cm)	I_{rel} (%)		$\frac{\nu}{\lvert\eta\rvert}$	$\frac{qS}{\eta}$	new p_{eff} (D)	old p_{eff} (D)
14	63.1	7.0±2.0	6.0	5±2	B′	3.97	1.0	5.7	5.6
		16.5±0.3	4.3	85±5	B				
		27.0±2.0	8.0	10±3	C				
	23.1	0.5±0.5	10.0	86±6	C′	1.45	1.0	—	—
		14.0±2.0	9.0	14±6	C				
	9.04	6.9±0.5	7.0	93±3	C	0.57	1.0	—	—
		20.4±2.0	8.0	7±3	D				

where B disappears. At X-band (9 GHz) two signals C and D are found. Signal C is sometimes split into C and C′.

In Table 2 results from measurements [14] with isotopically enriched Li^6 are listed. The assignments are similar to those made for the Li^7 spectra, however the Li^6 tunneling parameter is larger by a factor of 1.4 and therefore signal A disappears at 70 GHz and signal B at 32 GHz.

2.2. *Calculated ⟨100⟩ Spectra*

The diagrams shown in Fig. 2 a and b represent calculated isofrequency spectra corresponding to the observed spectrum in Figure 2 c. The strain parameter $|qS/\eta|$ is taken as abscissa, covering the range from 0 to 3. Figure 2 a shows that signals A and C start out with zero intensity, but gain relative intensities of more than 10 percent as the strain increases. At the same time signals A and C are shifted away from B as shown in Figure 2 b. This permits the evaluation of the strain parameter by comparison with the observed line positions of Fig. 2 c with the result $|qS/\eta| = 2$. Because of possible saturation [9] of the B signal in this particular spectrum, the relative intensities are unreliable and hence can not be used to obtain the strain parameter.

While Fig. 2 is restricted to a single frequency (72 GHz) the diagram in Fig. 3 shows results for all frequencies between 0 and $8|\eta|$, which covers the range from 0 to 90 GHz for Li^7 and 0 to 130 GHz for Li^6. The exclusive use of normalized units makes Fig. 3 independent of the absolute values for the tunneling parameter and the electric dipole moment. For a given frequency the calculated line positions are indicated by the curves in Figure 3. For zero strain there is only one curve, the solid line B (cf. Figure 1). For $|qS/\eta| = 1$, 2 and 3 different sets of curves give the respective line positions. It can be seen that signals A, B and C split into components when the frequency decreases. At high frequencies the A, B and C curves run parallel i. e. the spacing between these signals in the spectrum is independent of frequency. The asymptotic line spacing is $|\eta/p|$ plus the strain-induced shift, which is 6, 30 and 67 percent for $|qS/\eta| = 1$, 2 and 3 respectively. A spacing of $|\eta/p|$ is equal to one normalized unit in Figs. 2 b and 3 corresponding to 6.5 kV/cm for Li^7 and 9.6 kV/cm for Li^6. Good agreement with the experimental B – C spacing of 7.7 and 8.3 kV/cm for Li^7 (at 63 and 72 GHz, see Table 1) and 10.5 kV/cm for Li^6 (at 63 GHz, see Table 2) is obtained, when the strain shifts are taken into account. This demonstrates the posibility to determine the zero field splitting from the line spacing in the high frequency ⟨100⟩ spectrum.

Figure 4 is closely related to Figure 3. Here are plotted the total (Fig. 4 a) and relative (Fig. 4 b) transition probabilities as calculated for the isofrequency spectra of Figure 3. The peaks in Fig. 4 a are of particular interest in connection with the frequency sweep low field PER experiment [8]. Whenever a curve for an intense line intersects at zero field in Fig. 3 a peak in the total intensity curve of Fig. 4 a appears. Experimentally [8] these peaks occur at 9, 15, and 22.2 GHz for Li^7 and at 9, 24 and 31.5 GHz for Li^6 (see also App. II).

Figure 4 b clearly shows that the D signal becomes unobservable at higher frequencies, therefore the D curves in Fig. 3 have been truncated. For very low frequencies no calculated curves are shown in Figure 4 b. During calculation it was found that for these particular frequencies a reliable simulation of random strain would require more than the 13 directions used in the present work.

2.3. *Comparison between Experiment and Calculation for ⟨100⟩ Spectra*

Excellent agreement between the experimental points and the calculated curves in Figs. 3 and 4 b is obtained, when the strain parameter is properly adjusted. The two important aspects of this result are: i) The present strain calculations fully explain the observed spectra; ii) Experimental parameters including random strain can be obtained from a comparison with the calculated curves.

In Tables 1 and 2 values for the electric dipole moment and for the strain parameter are listed. The tunneling parameters were considered fixed parameters because the very accurate values $\eta(Li^7) = -11.1$ and $\eta(Li^6) = -15.9$ GHz are available from the literature [8]. They replace the approximate values of -10 and -14 GHz used in I.

Since the position of the main B signal is insensitive to internal strains, Eq. (1) has been used to redetermine the electric dipole moment. The average of the six values in Table 1 yields $p_{eff}(Li^7) = 5.9$ Debye and the value in Table 2 is $p_{eff}(Li^6) = 5.7$ D. For comparison the values derived from the same spectra by the original authors are given in the last column of Tables 1 and 2. Differences arise mainly from different assumed values for η.

For the strain parameter $|qS/\eta|$ values between 1.0 and 2.5 are obtained. They can be related to differences in sample preparation, which will be discussed in Section 5.1.

3. PER for the ⟨110⟩ Orientation

Seven experimental spectra from Li^7 have been reported for the ⟨110⟩ orientation. There are none for Li^6. The calculated spectra predict up to six lines which are only partly resolved experimentally.

3.1. *Observed ⟨110⟩ Spectra*

Table 3 gives data on experimental ⟨110⟩ spectra from published [3, 4, 14, 15] or thesis [16, 17] work. The organization of Table 3 is similar to that of Table 1 and the explanations given in Section 2.1 apply also here.

Table 3. Data on ⟨110⟩ PER spectra of KCl: Fi^7

Ref.	Experiment				Assignment	Analysis		
	ν (GHz)	$c \cdot F$ [a] (kV/cm)	$2W_h$ [a] (kV/cm)	I_{rel} (%)		$\frac{\nu}{\lvert\eta\rvert}$	$\frac{qS}{\eta}$	p_{eff} (D)
15	35.0	10.3±0.5	10.0	97±2	B	3.15	1.1	6.2
		(23±2))	(7)	3±2	C			
14	64.0	8.8±1.0	6.0	3±2	A′	5.77	1.25	5.9
		(20±2)			B′			
		25.0±1.0	15.0	94±4	B°			
		(31±3)			B″			
		39.0±3.0	8.0	3±2	C			
17	29.1	7.8±0.6	10.2	96±2	B	2.62	2.5	6.0
		(22±2)		4±2	C			
16	36.63	13.5±1.0	11.3	96±2	B	3.30	1.7	5.2
		(28±2)		4±2	C			
3	34.7	12.0±0.5	8.4	96±2	B	3.13	2.0	5.8
		(25±3)		4±2	C			
	9.3	1.7±0.4	4.6	35±8	C″	0.84	2.0	—
		5.8±0.6	5.8	46±8	C′			
		10.0±1.0	8.6	19±9	C°			
4	74.2	12.0±1.0	6.5	6±3	A′	6.68	2.0	5.2
		(16.5±2)	(13)		A°			
		(26±3)			B′			
		33.0±1.0	13.0	92±4	B°			
		(40±3)			B″			
		49.5±2.0	(6)	2±1	C			
						Average $p_{eff} = 5.7$		

[a] Numbers in parenthesis are less certain.

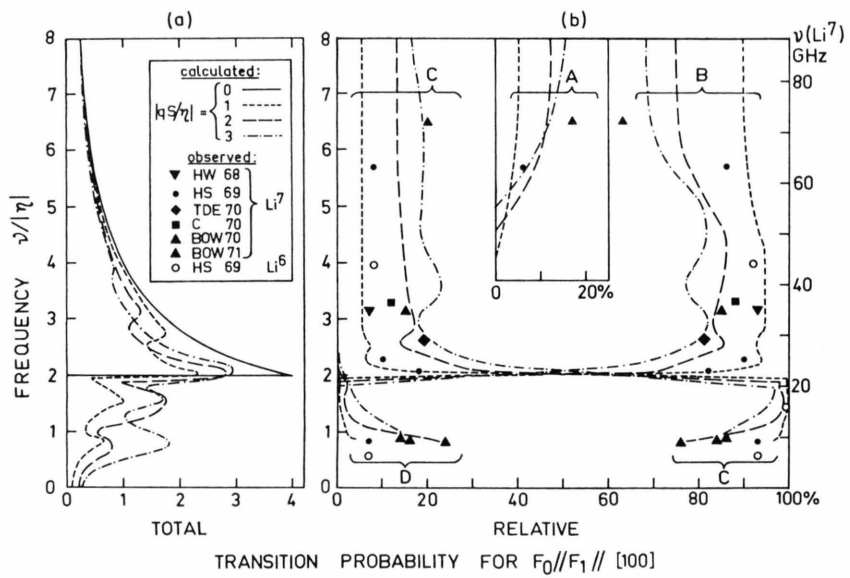

Fig. 4.

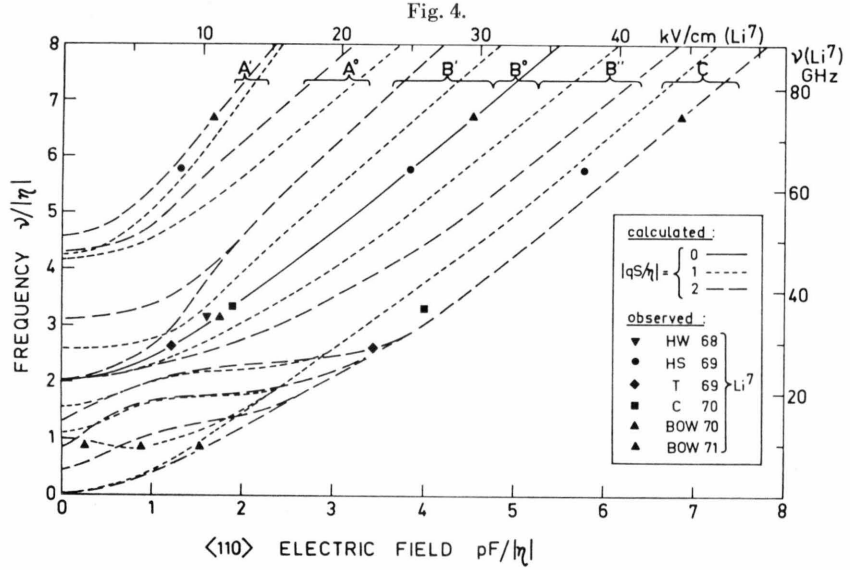

Fig. 6.

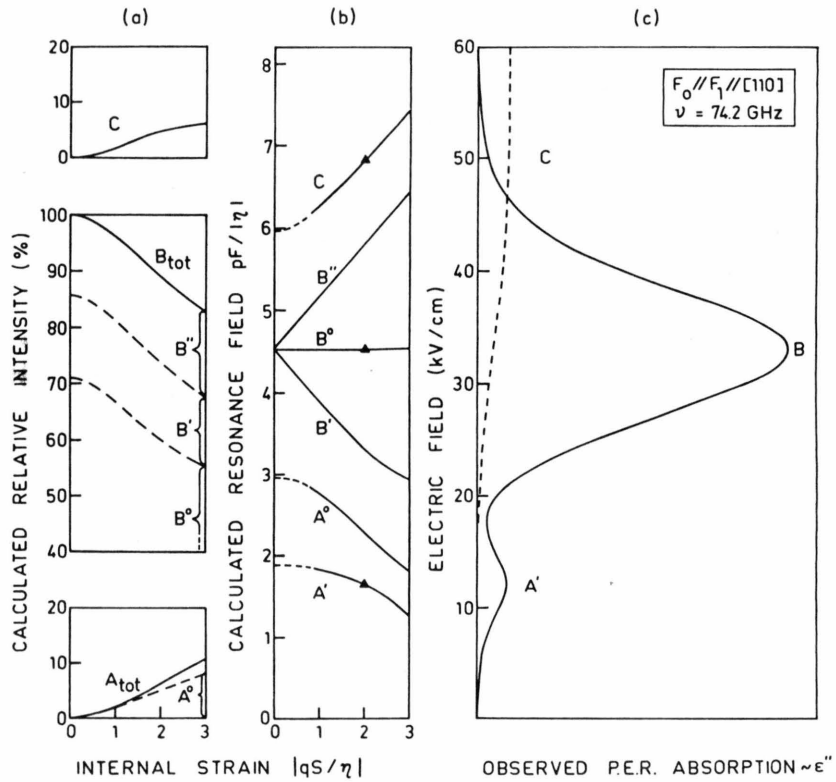

Fig. 5.

Fig. 5. (a) Calculated relative intensities for the PER signals of Fig. 5 b and their dependence on the strain parameter $|qS/\eta|$. Note that $A_{tot}=A^0+A'$ and $B_{tot}=B^0+B'+B''$.
(b) Calculated line positions for a ⟨110⟩ PER spectrum as a function of the strain parameter $|qS/\eta|$. The vertical scale coincides with that of Fig. 5 c. The normalized frequency is $\nu/|\eta|=6.68$.
(c) Experimental ⟨110⟩ PER absorption spectrum after Blumenstock, Osswald, and Wolf [4] at 74.2 GHz. The broken line represents the "background" signal.

Fig. 4. Calculated transition probabilities and observed relative intensities for ⟨100⟩ PER spectra, plotted as a function of frequency. The curves were calculated using values of 0, 1, 2, and 3 for the strain parameter $|qS/\eta|$. (a) Total calculated transition probability. No experimental points are available but the peak position correlate with those observed in a special PER experiment [8]. (b) Relative intensities (in %) of signals A, B, C, and D within the ⟨100⟩ PER spectrum. Experimental points are given according to Tables 1 and 2. The symbols and abbreviations have the same meaning as in Figure 3.

Fig. 6. Frequency versus fiel diagram for ⟨11⟩ PER spectra showing calculated and observed line positions for KCl : Li. The left and bottom scale are in normalized units allowing general use of the diagram for systems with ⟨111⟩ dipoles. The corresponding absolute units on the right and top scale are for Li^7 only. The curves were calculated using values of 0, 1, and 2 for the strain parameter $|qS/\eta|$. They are labelled A′, A^0, B′, B^0, B″ and C from left to right. Experimental points are given according to Table 3. The abbreviations in the insert have the following meaning: HW 68 = [15], HS 69 = [14], T 69 = [17], C 70 = [16], BOW 70 = [3], BOW 71 = [4].

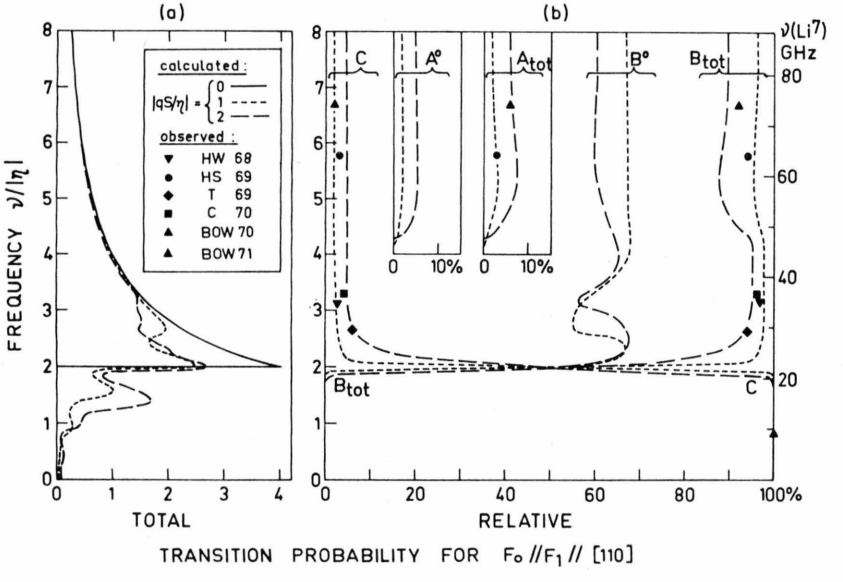

Fig. 7. Calculated transition probabilities and observed relative intensities for ⟨110⟩ PER spectra, plotted as a function of frequency. The curves were calculated using values of 0, 1, and 2 for the strain parameter $|qS/\eta|$. (a) Total calculated transition probability. No experimental points are available. (b) Relative intensities (in %) of signals A^0, A_{tot}, B^0, B_{tot}, and C within the ⟨110⟩ PER spectrum, where $A_{tot}=A^0+A'$ and $B_{tot}=B^0+B'+B''$. Experimental points are given according to Table 3. The symbols and abbreviations have the same meaning as in Figure 6.

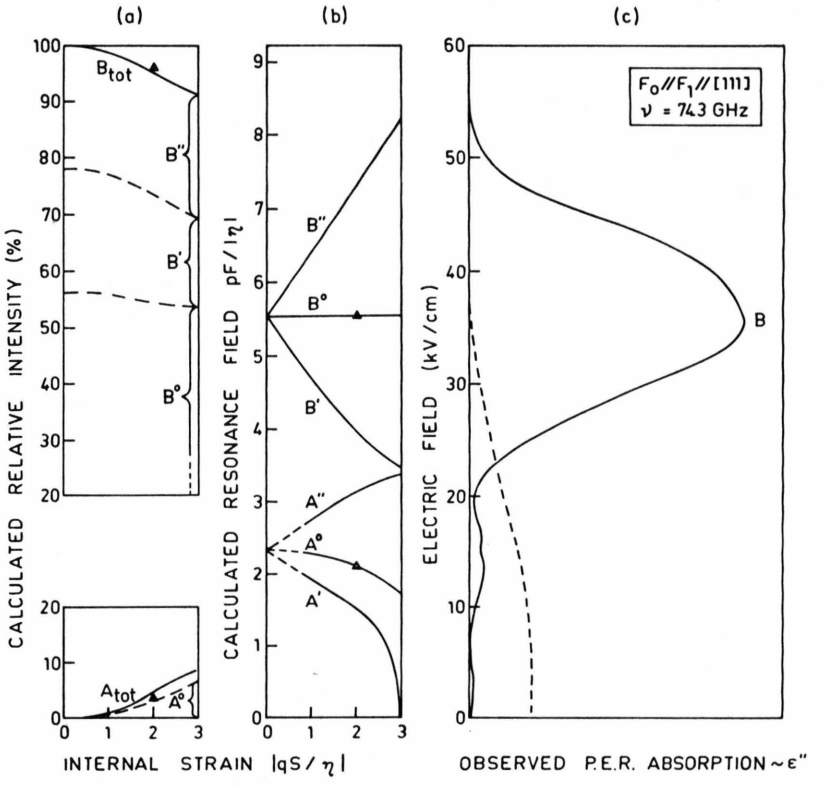

Fig. 8. (a) Calculated relative intensities for the PER signals of Fig. 8 b and their dependence on the strain parameter $|qS/\eta|$. Note that $A_{tot}=A^0+A'+A''$ and $B_{tot}=B^0+B'+B''$.
(b) Calculated line positions for a ⟨111⟩ PER spectrum as a function of the strain parameter $|qS/\eta|$. The vertical scale coincides with that of Figure 8 c. The normalized frequency is $\nu/|\eta|=6.69$.
(c) Experimental ⟨111⟩ PER absorption spectrum after Blumenstock, Osswald, and Wolf [4] at 74.3 GHz. The broken line represents the "background" signal.

Figure 5 c shows a typical ⟨110⟩ spectrum. Unfortunately there is considerable overlap of lines which makes the analysis a difficult task. The main signal B consists of the unresolved components B′, B°, and B″. The A and C signals are substantially weaker than for the ⟨100⟩ orientation. The A signal disappears [7] at zero field around 50 GHz. The C signal is not well separated from the B triplet. Below 22 GHz the B signal has disappeared and at 9.3 GHz the spectrum consists of the C signal only, which is now split into components C°, C′, and C″.

3.2. Calculated ⟨110⟩ Spectra

The diagrams in Fig. 5 a and b represent calculated spectra corresponding to the observed spectrum in Figure 5 c. From Fig. 5 b it can be seen that signal B splits into three components B′, B°, and B″. The splitting is proportional to the strain parameter. The intensities of the components have the approximate ratio 1 : 5 : 1, as shown in Figure 5 a.

The strain parameter for the experimental spectrum in Fig. 5 c can be obtained by fitting the positions and relative intensities of lines A′ and C to the calculated curves. The result $|qS/\eta| = 2$ is supported by the more accurate value obtained from the corresponding ⟨100⟩ spectrum.

The complete calculated results for the ⟨110⟩ orientation are presented in Figs. 6 and 7. The diagrams cover the range 0 – 90 GHz for Li^7 and 0 – 130 GHz for Li^6. In order to avoid disturbing overlap, the curves for $|qS/\eta| = 3$ are not shown, however linear extrapolation can be used, see Fig. 5 a and b. At high frequencies, curves A°, B°, and C in Fig. 6 run parallel. The asymptotic spacing is $\sqrt{2}\,|\eta/p|$ plus the strain induced shift, which is 20, 60 and 104 percent for $|qS/\eta| = 1$, 2, and 3 respectively. With increasing frequency the intensity of signal A′ goes to zero and its position develops into a half field resonance, as indicated by the different slope in Figure 6. Also signal A′ is relatively sharp because for moderate strain its position is almost strain-independent (see Figure 5 b).

3.3. Comparison between Experiment and Calculation for the ⟨110⟩ Spectra

Very good agreement between the experimental points and the calculated curves in Figs. 6 and 7 b is obtained, if the proper strain parameter is used. These values are given in Table 3. Under the assumption, that the observed maximum of the B absorption signal coincides with the B° line, the electric dipole moment has been determined, using Equation (1). The averaged value, $p_{\text{eff}} = 5.7$ Debye is very close to the value 5.9 obtained from the ⟨100⟩ spectra in Section 2.3. The small difference is within experimental error, however the possibility of a true anisotropy in p_{eff} (e. g. from the KCl antishielding) cannot be ruled out especially since a similar difference was found in the infrared study [10], i. e. 5.47 D for ⟨100⟩ and 5.33 D for ⟨110⟩.

4. PER for the ⟨111⟩ Orientation

For the ⟨111⟩ orientation six complete experimental spectra have been reported for Li^7 and none for Li^6. The calculated spectra predict up to six lines, which are only partly resolved experimentally. Misorientation of the sample may cause additional line splitting, since the ⟨111⟩ direction is a crossover point in the angular dependence [2].

4.1. Observed ⟨111⟩ Spectra

Table 4 summarizes data on the experimental ⟨111⟩ spectra from published [3, 4, 15] or thesis [16, 17] work. Included are five spectra taken at frequencies between 60.1 and 72.4 GHz, where only the low field part has been reproduced [4].

Figure 8 c shows a typical ⟨111⟩ spectrum. The main B signal is an unresolved triplet as in the ⟨110⟩ case. There is no high field C line. The A signal disappears [7] at zero field around 50 GHz. Only part of the B signal disappears at 22 GHz; the remainder can be observed as a low field line down to X-band frequencies. In the 9.3 GHz spectrum this line is located at 1.8 kV/cm, partly overlapping with the much broader high field line D at 8 kV/cm. This D line occurs at 25 kV/cm in the 29.1 GHz spectrum.

4.2. Calculated ⟨111⟩ Spectra

The diagrams in Fig. 8 a and b represent calculated spectra corresponding to the experimental spectrum in Figure 8 c. The splitting of the B signal into three components B′, B°. and B″ is almost linear with the strain parameter. The intensities of the B components have the approximate ratio 2 : 5 : 2 (see Figure 8 a). The A signal, which starts

Table 4. Data on ⟨111⟩ PER spectra of KCl: Li^7.

Ref.	Experiment				Assignment	Analysis		
	ν (GHz)	$c \cdot F$ [a] (kV/cm)	$2W_h$ (kV/cm)	I_{rel} (%)		$\frac{\nu}{\lvert\eta\rvert}$	$\frac{qS}{\eta}$	p_{eff} (D)
15	35.0	6.0±1.0	6.0	—	Li^6	2.20	—	—
		13.3±0.5	14.4	100	B	3.15	1.1	6.1
17	29.1	9.8±0.5	9.5	94±3	B	2.62	2.5	5.7
		25.0±2.0	9.0	6±3	D			
16	36.43	8.2±1.0	4.0	—	Li^6	2.29	—	—
		15.6±0.5	13.0	100	B	3.28	1.7	5.5
3	34.7	6.3±1.0	4.0	—	Li^6	2.18	—	—
		13.2±0.5	8.8	100	B	3.13	2.0	6.0
	9.3	1.8±0.5	5.0	28±5	B	0.84	2.0	—
		8.0±1.0	14.4	72±5	D			
4	74.3	3.3	4.0	—	Li^6	4.67	—	—
		10.0	3.0	4±2	A′	6.69	2.0	5.9
		13.8	6.0		A°			
		(29±3)			B′			
		35.5±1.0	16.0	96±2	B°			
		(43±3)			B″			
	72.4	4.0±2.0	4.0	—	Li^6	4.55	—	—
		9.0±3.0	4.0	—	A′	6.52	2.0	—
		13.0±3.0	6.0	—	A°			
		20.0±3.0	3.0	—	A″			
	68.1	0.0±1.0	5.0	—	Li^6	4.28	—	—
		6.0±2.0	5.0	—	A′	6.14	2.0	—
		11.0±3.0	7.0	—	A°			
		19.0±3.0	3.0	—	A″			
	67.2	5.0±2.0	6.0	—	A′	6.05	2.0	—
		11.0±3.0	6.0	—	A°			
		18.0±2.0	4.0	—	A″			
	65.0	2.5±2.0	6.0	—	A′	5.85	2.0	—
		10.0±2.0	6.0	—	A°			
		17.0±2.0	5.0	—	A″			
	60.1	8.0±3.0	6.0	—	A°	5.41	2.0	—
		14.0±2.0	6.0	—	A″			

Average p_{eff}=5.8

[a] Numbers in parenthesis are less certain.

out with zero intensity, also splits into three components A′, A°, and A″, which are related to strain of different symmetry as discussed later (see Section 5.4 and App. I).

The complete calculated results for the ⟨111⟩ orientation are given in Figs. 9 and 10. There is no C signal in contrast to the ⟨100⟩ and ⟨110⟩ cases. A new feature is the additional B signal branch below $\nu/|\eta| = 2$, which does not exist in the presence of a C signal, due to some sort of "repulsion" effect.

At high frequencies, the group of A signals occurs at half the field of the B signals and the A signal intensity goes to zero. The position of A° becomes strain-independent, similar to B°. A new detail in Fig. 10 a is the increase of total transition probability by internal strain around $\nu/|\eta| = 3$, which is due to zero field intercepts of intense B signal components in Figure 9.

4.3. Comparison between Experiment and Calculation for the ⟨111⟩ Spectra

Very good agreement between the experimental points and the calculated curves in Figs. 9 and 10 b is obtained if the strain parameter is properly adjusted. These values are given in Table 4. For the three spectra, taken at frequencies between 34.7 and 36.4 GHz, the fitting procedure is almost impossible because only the unresolved B triplet is observed (the weak low field line being due to Li^6). The series of spectra in the 60 to 75 GHz range provides

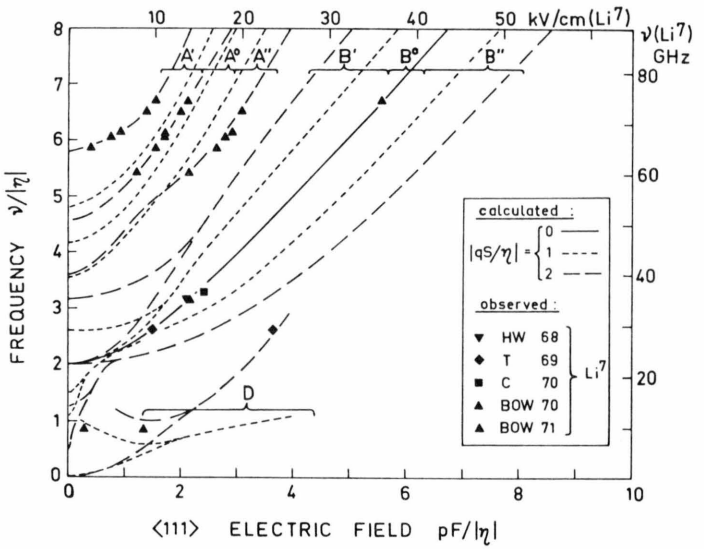

Fig. 9. Frequency versus field diagram for ⟨111⟩ PER spectra showing calculated and observed line positions for KCl : Li. The left and bottom scale are in normalized units allowing general use of the diagram for systems with ⟨111⟩ dipoles. The corresponding absolute units on the right and top scale are for Li^7 only. The curves were calculated using values of 0, 1, and 2 for the strain parameter $|qS/\eta|$. They are labelled A′, A^0, A″, B′, B^0, and B″ from left to right. Experimental points are given according to Table 4. The abbreviations in the insert have the following meaning: HW 68 = [15], T 69 = [17], C 70 = [16], BOW 70 = [3], BOW 71 = [4].

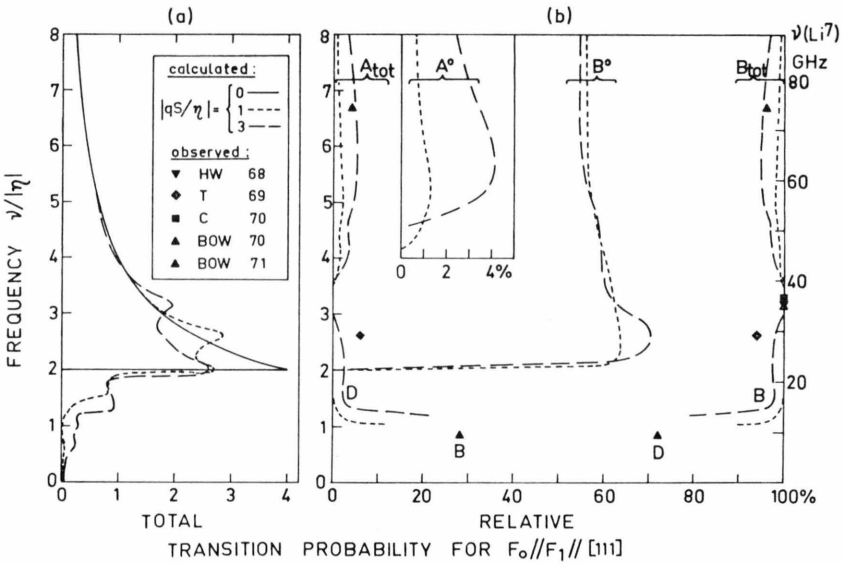

Fig. 10. Calculated transition probabilities and observed relative intensities for ⟨111⟩ PER spectra, plotted as a function of frequency. The curves were calculated using values of 0, 1, and 2 for the strain parameter $|qS/\eta|$.

(a) Total calculated transition probability. No experimental points are available.

(b) Relative intensities (in %) of signals A^0, A_{tot}, B^0 and B_{tot} within the ⟨111⟩ PER spectrum ,where $A_{tot}=A^0+A'+A''$ and $B_{tot}=B^0+B'+B''$. Experimental points are given according to Table 4. The symbols and abbreviations have the same meaning as in Figure 9.

Table 5. Dependence of internal strain and electric field on sample preparation for KCl: Li^7.

Ref.	Preparation method	Strain			Field		
		$\frac{qS}{\eta}$	qS (GHz)	S (bar)	F [a] (kV/cm)	$2pF$ (GHz)	$\frac{pF}{\lvert\eta\rvert}$
15	Kyropoulos (seed pulled)	1.1	12	18	4.4	15	0.68
14	Kyropoulos (seed pulled)	1.25	14	21	3.5	12	0.54
2, 17	Harshaw with subsequent Li-diffusion	2.5	28	42	4.3	15	0.66
16	Harshaw, melt doped	1.7	19	28	3.7	13	0.57
3, 4	Zone refined	2.0	22	33	2.3	8	0.35

[a] Obtained from ⟨100⟩ B signal, where $F=W_h\cdot\sqrt{2}$,

a remarkable test on the accuracy of the calculations. The surprisingly close agreement leads to the conclusion, that inherent limitations imposed by the assumptions and simplifications in the present calculation are of minor importance. The averaged dipole moment from Table 4 is $p_{\text{eff}} = 5.8$ Debye.

5. Discussion

5.1. *Influence of Sample Preparation*

Inspection of Tables 1, 3, and 4 shows that the fitted internal strain parameter $|qS/\eta|$ for Li^7 depends on sample preparation but not on the frequency or orientation at which the PER spectra were taken. Accordingly the relevant strain data are rearranged in Table 5. For the conversion of normalized $|qS/\eta|$ units into GHz the tunneling parameter $\eta = -11.1$ GHz is used. The corresponding stress in bar units is obtained by inserting the elastic moment $q = 0.674$GHz/bar (see I and Ref. [6]; recently [5] a slightly larger value of $q = 4\,\text{K} = 0.74 \pm 15\%$ GHz/bar was obtained from uniaxial stress effects in PER spectra). In one case (not listed in Table 5) sample quality could be improved by after-growth treatment [5]. Vacuum annealing at 400 °C combined with slow cooling down to helium temperature reduced the width of the B signal in the ⟨110⟩ spectrum at 64.5 GHz by a factor of two. From the position and relative intensity of the A signal in the annealed-sample spectrum a reduction of internal strain by 20 – 30% can be estimated.

5.2. *Apparent PER linewidth and Internal Electric Fields*

All experimental lines were analyzed for their apparent halfwidth, $2W_h$, as listed in Tables 1 to 4. In Figure 11 the B signal walfwidth is plotted as a function of frequency for the ⟨100⟩, ⟨110⟩, and ⟨111⟩ orientation. For ⟨100⟩ the calculations predict a single unsplit B line. The observed linewidth is relatively small and shows no variation with frequency. However, the PER halfwidth found in zone-refined samples is consistently smaller than in seed-pulled samples (see Table 5). It is well known that zone refining reduces internal electric fields. This leads to the conclusion that the halfwidth of the B line in the ⟨100⟩ spectrum can be used as a measure for random internal electric fields. In the ⟨110⟩ and ⟨111⟩ spectra the B signals are unresolved triplets.

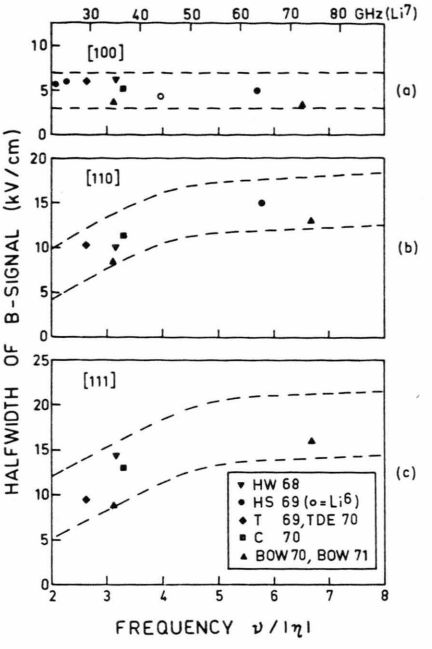

Fig. 11. Apparent halfwidth $2W_h$ of the B signal plotted as a function of frequency. The bottom scale is in normalized units and the corresponding absolute units for Li^7 are given on the top scale. The fields F_0 and F_1 are oriented along a) [100], b) [110], and c) [111]. Experimental points are given according to Table 1, 2, 3, and 4. The abbreviations in the insert have the following meaning: HW 68 = [15], HS 69 = [14], T 69 = [17], TDE 70 = [2], C 70 = [16], BOW 70 = [3], BOW 71 = [4]. The calculated broken lines give the expected lower and upper limits if the following holds: i) The [100] signals are broadened by random internal fields only. ii) The corresponding values for [110] and [111] are obtained by multiplication with $\sqrt{2}$ and $\sqrt{3}$, respectively. iii) The additional frequency dependent broadening for [110] and [111] is due to the unresolved triplet structure of the B signal and is taken into account by using the B′ to B″ spacing in Figs. 6 and 9 for $|qS/\eta| = 2$ and multiplying by an (empirical) factor of 0.4.

The curves in Fig. 11 b and c have been derived from the B′ to B″ spacings in Figs. 6 and 9 to which the random electric field induced width according to Fig. 11 a has been added. The agreement with the experimental points is good if an isotropic distribution of internal electric field directions is assumed, i. e. the intercepts at $\nu = 2|\eta|$ have the ratio $1 : \sqrt{2} : \sqrt{3}$ for the ⟨100⟩, ⟨110⟩, and ⟨111⟩ orientation. For this frequency the strain induced triplet splitting vanishes both theoretically and experimentally, the remaining linewidth being due to the internal electric fields.

5.3. *Profile for the Magnitude of Internal Strains*

So far, the simplifying assumption has been made that the magnitude of the random internal strains

can be represented by a single value of the strain parameter $|qS/\eta|$. For Li in KCl it is expected that the probability for zero strain is small and for very large strain goes to zero. Thus the strain profile should have a maximum at some intermediate strain magnitude and fall off to both sides. For the theoretical profile a Gaussian is assumed, characterized by the sharpness parameter $S_0/\delta S$, where the maximum occurs at S_0 and $2\,\delta S$ is the full width at half height (see Figure 12 c).

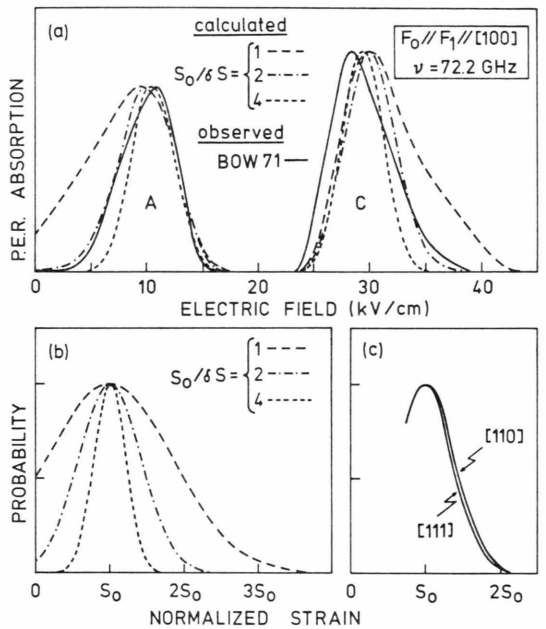

Fig. 12. (a) Comparison of observed and calculated signal shapes for the A and C signal in the ⟨100⟩ spectrum at 72.2 GHz. The observed curves (solid lines) are those of Figure 2 c. The calculated curves (broken lines) are for the strain profiles of Fig. 12 b and the vertical scale has been adjusted to the observed peak height of the A and C signal, respectively. (b) Gaussian profiles for the strain magnitude with three different values for the sharpness parameter $S_0/\delta S$, where S_0 is the abscissa of the peak and $2\,\delta S$ is the full width at half height.
(c) Strain profile obtained from the B′ and B″ signal components in the ⟨110⟩ and ⟨111⟩ spectrum of Figs. 5 and 8. The procedure is described in the text and due to overlap with the central B° component, the left part of the profile is less certain.

In order to derive a quantitative result from the observed PER spectra, the following procedure was chosen. Theoretical curves for the A and C signal in the 72.2 GHz ⟨100⟩ spectrum (cf. Figure 2) were constructed using different profiles for the strain magnitude: Calculated spectra for different values of $|qS/\eta|$ were superimposed, where the statistical weights and the broadening from random electric fields have been taken into account. As shown in Fig. 12 a only the narrow profile with $S_0/\delta S = 2$ leads to a good fit.

An independent but similar result is obtained from the B′ and B″ line shapes in the ⟨110⟩ and ⟨111⟩ spectra of Figs. 5 and 8. Since the B′ and B″ relative intensity is almost independent of strain, the strain profile can be directly obtained by subtracting B° and correcting for the random electric field induced broadening. The results are shown in Figure 12 c. The strain profile is very close to a Gaussian and the value for $S_0/\delta S$ is slightly less than 2, in excellent agreement with the independent determination above.

The sharpness of the strain profile is a very interesting result, which will be further treated in Sections 5.5 and 6.

5.4 Isotropy of Strain Direction

The 13 stress directions which simulate the random strains differ in symmetry, being tetragonal for the ⟨100⟩, orthorhombic for the ⟨110⟩ and trigonal for the ⟨111⟩ orientation. The corresponding statistical weights are 27%, 45%, and 28% for isotropic strain (see I). In the calculated PER spectra individual lines are related to stress of particular symmetry. This relationship can be used to examine the observed PER spectra with respect to strain anisotropy. For example in the high frequency ⟨111⟩ spectrum (cf. Fig. 8) the intensity of the B° line is determined by the tetragonal (and zero) stress, that of the A° line by orthorhombic stress, and that of the A′ and A″ lines by the trigonal stress. Similar relations hold for the other spectra (see App. I).

The best agreement between calculated and observed intensities is obtained under the assumption of isotropic strain. Thus no preferred strain direction is found at the sites of the paraelectric Li in KCl. As discussed in I, the host material may be divided into moderately strained regions where the "normal" Li is found, and highly strained regions (close to the ⟨110⟩ edge dislocation lines) where the Li becomes "anomalous". The above results are restricted to the "normal" regions of KCl.

5.5. Paraelectric Li in KCl as a Microprobe

As shown in the preceeding sections, random internal strains and random electric fields can be determined by careful analysis of the PER spectra

(see Table 5). Thus, paraelectric lithium has the properties of a microprobe. It is important to note that the natural content of 0.01 to 0.1 ppm Li in nominally pure KCl is sufficient, since PER is a very sensitive spectroscopic method.

For this microprobe application, estimated data for the suitable range and the accuracy are collected in Table 6. The first and the last line are easily obtained from Table 5 by extrapolation of the actually observed values within reasonable limits. The second line is related to the parameter α, which was defined in I. In general, internal strain will contain stress components of A_{1g}, E_g, and T_{2g}

Table 6. Paraelectric Li as a microprobe.

Crystalline perturbation	Suitable range	Estimated error
Internal strains (T_{2g}-Component)	10—200 bar	10—30%
Internal strains (A_{1g}, E_g-Components)	100—1000 bar	20—50%
External hydrostatic pressure (A_{1g})	100—7000 bar	—
Internal electric fields	1—20 kK/cm	20—50%

symmetry (see I), but only the T_{2g} components can interact with the elastic moment of the off-center Li. The other components modify the tunneling parameter η by very small amounts and are therefore not detectable below 100 bar.

It should be emphasized that Table 6 refers to Li at the "normal" sites mentioned in Section 5.4. The very high strains at dislocation lines can cause the lithium ions to loose part or all of their paraelectric properties; therefore these sites are called "anomalous", allowing no normal PER.

The last line in Table 6 refers to an experiment, where the effect of applied hydrostatic pressure has been studied with far infrared spectroscopic methods [19]. The tunneling splitting increases exponentially with pressure and becomes stationary at 7 kbar, indicating that the lithium has approached the "one-site" position in the lattice [19].

6. Conclusions

The present results may be summarized as follows: (i) A new level of understanding has been reached by the complete and satisfactory interpretation of the observed PER spectra of Li in KCl. (ii) Using the calculated data, values for random internal strain and random internal electric field have been determined. (III) The profile of the distribution of strain magnitudes is found to be very narrow.

The quantitative results on the strain statistics may be of particular interest in connection with averaging phaenomena in the electron paramagnetic resonance spectra of Jahn-Teller systems. There, the indication of a well defined relaxation rate, i.e. a narrow profile of the strain magnitude, has been implied by the interpretation of relaxation effects [20].

Appendix I

Special Effects from Anisotropic Strain

In Section 5.4 the isotropy of strain direction in KCl was established by the fact that special effects from anisotropic strain were absent. Such special effects can be easily predicted from the present cal-

Table 7. Effects of anisotropic strain on the relative intensities.

Spectrum	Type of strain	Relative intensities (%)						
		A′	A°	A″	B′	B°	B″	C
⟨100⟩	isotropic	—	12	—	—	75	—	13
	tetragonal	—	0	—	—	100	—	0
	orthorhombic	—	18	—	—	63	—	19
	trigonal	—	20	—	—	58	—	22
⟨110⟩	isotropic	1	5	—	14	60	15	5
	tetragonal	0	0	—	0	100	0	0
	orthorhombic	2	7	—	17	50	17	7
	trigonal	0	7	—	24	39	25	5
⟨111⟩	isotropic	0.5	2	0.5	21	54	22	—
	tetragonal	0	0	0	0	100	0	—
	orthorhombic	0	4	0	32	32	32	—
	trigonal	1.5	2	1.5	21	50	24	—

culations. The dominant effects show up in the relative intensities of different lines in the spectrum. Changes in the line positions are very small and will not be discussed.

In Table 7 data for the following strain cases are given: (i) isotropic strain, (ii) all strain is tetragonal and equally distributed over the three ⟨100⟩ axes, (iii) all strain is orthorhombic and equally distributed over the six ⟨110⟩ axes, (iv) all strain is trigonal and equally distributed over the four ⟨111⟩ axes. The application of external uniaxial stress constitutes still another case, which will be treated separately [6].

The strain magnitude was chosen to be $|qS/\eta| = 2$ and the frequency $\nu = 8|\eta|$. The special effects listed in Table 7 are valid for a wide frequency range and can be applied to the experimental high frequency PER spectra, especially those in Figs. 2, 5, and 8.

Appendix II

Paraelectric Resonance of RbCl : CN

In a recent dielectric susceptibility investigation [21] it was suggested, that the electric dipole of the CN^- molecular impurity in RbCl points in a ⟨111⟩ direction, contrary to earlier interpretations including the PER spectra [22] of this system. A preliminary inspection of the published [22] PER spectra indeed favours the ⟨111⟩ model very strongly. The forbidden transitions are readily assigned from Figs. 3, 6, and 9. However, these spectra were taken at frequencies very close to the "ideal" zero field splitting $|2\eta|$, where the forbidden transitions exhibit a rather complex behaviour. Details will be given in a separate quantitative treatment [23].

In connection with the ⟨111⟩ model for RbCl:CN a calculation on the effects of internal strains has been performed [21], similar to that given in I. Using a Monte-Carlo random-number technique a curve which resembles Fig. 4 a of the present paper was obtained. In spite of the different meaning of the curves (Fig. 4 a is for the total isofrequency spectrum, whereas Fig. 7 of Ref. [21] is for zero static electric field) a comparison can be made. At frequencies lower than the "ideal" zero field splitting $|2\eta|$ the present calculation yields two absorption humps in excellent agreement with experiments (see Fig. 3 and Ref. [8]). For RbCl: CN only one hump is obtained [21] experimentally and from the calculation, which may be a wash-out effect.

Acknowledgments

The author is indebted to T. L. Estle, R. H. Silsbee, H. S. Sack, and R. Osswald for valuable discussions. R. W. Timme and J. G. Carnes kindly permitted to include their unpublished PER results in the present analysis. Useful comments on the manuscript by J. R. Herrington and O. F. Schirmer are gratefully acknowledged.

[1] B. Dischler, Z. Naturforsch. **25 a**, 1844 [1970].
[2] a) T. L. Estle, B. Dischler, and R. W. Timme, Bull. Amer. Phys. Soc. **14**, 346 [1969]. b) R. W. Timme, B. Dischler, and T. L. Estle, Phys. Rev. **B 1**, 1610 [1970].
[3] D. Blumenstock, R. Osswald, and H. C. Wolf, Z. Physik **231**, 333 [1970].
[4] D. Blumenstock, R. Osswald, and H. C. Wolf, Phys. Stat. Sol. **B 46**, 217 [1971].
[5] T. R. Larson and R. H. Silsbee, Phys. Rev. **B 5**, 778 [1972].
[6] B. Dischler, to be published.
[7] A. V. Frantsesson, O. F. Dudnik, and V. B. Kravchenko, Fizika Tverdogo Tela **12**, 160 [1970]. English translation: Soviet Phys. Sol. State **12**, 126 [1970].
[8] W. G. Von Holle, J. S. H. Wang, R. S. Scott, and W. H. Flygare, Solid State Comm. **8**, 1363 [1970].
[9] R. Osswald and H. C. Wolf, Phys. Stat. Sol. **B 50**, K 93 [1972].
[10] R. D. Kirby, A. E. Hughes, and A. J. Sievers, Phys. Rev. **B 2**, 481 [1970].
[11] a) S. P. Bowen, M. Gomez, J. A. Krumhansl, and J. A. D. Matthew, Phys. Rev. Letters **16**, 1105 [1966]. b) M. Gomez, S. P. Bowen, and J. A. Krumhansl, Phys. Rev. **153**, 1009 [1967].
[12] T. L. Estle, Phys. Rev. **176**, 1056 [1968].
[13] a) H. B. Shore, Phys. Rev. **151**, 570 [1966]. b) P. Sauer, O. Schirmer, and J. Schneider, Phys. Stat. Sol. **16**, 79 [1966].
[14] R. A. Herendeen and R. H. Silsbee, Phys. Rev. **188**, 654 [1969].
[15] G. Höcherl and H. C. Wolf, Phys. Letters **27 A**, 133 [1968].
[16] J. G. Carnes, Ph.D.-Thesis, Rice University 1970 (unpublished).
[17] R. W. Timme, M.A.-Thesis, Rice University 1969 (unpublished).
[18] M. F. Deigen, M. D. Glinchuk, and V. S. Vikhnin, Fizika Tverdogo Tela **13**, 2714 [1971]. English translation: Sov. Phys. Sol. State **13**, 2270 [1972].
[19] A. M. Kahan and A. J. Sievers, Bull. Amer. Phys. Soc. **17**, 239 [1972].
[20] J. R. Herrington, T. L. Estle, and L. A. Boatner, Phys. Rev. **B 3**, 2933 [1971], **B 7**, 3003 [1973] and to published.
[21] R. R. Hayes and H. S. Sack, Phys. Rev. **B 6**, 599 [1972], additional references for RbCl: CN^- are given there.
[22] R. W. Dreyfus, J. Phys. Chem. Solids **29**, 1941 [1968].
[23] B. Dischler, to be published.